CENTERIS - International Conference on ENTERprise Information Systems / ProjMAN - International Conference on Project MANagement / HCist - International Conference on Health and Social Care Information Systems and Technologies 2020

OCLeaS – A tomographic PSI Algorithm using Orthogonal Matching Pursuit and Complex Least Squares

Matthieu Rebmeister*, Andreas Schenk, Patrick Erik Bradley, Nils Dörr, Stefan Hinz

Institute of Photogrammetry and Remote Sensing, Engessersraße 6, 76131 Karlsruhe, Germany

Abstract

This letter describes an algorithm using Compressive Sensing to analyse a stack of SAR images to monitor small urban areas. It uses the combination of the Orthogonal Matching Pursuit and Complex Least Squares, in order to estimate the residual height, thermal dilation coefficient and the displacement rate associated with one or multiple dominant persistent scatterers in a SAR resolution cell. It can be interpreted as a hybrid tomographic-PSI algorithm. The proposed method is tested with simulated data over single and double PS. Then it is applied to a stack of 79 SAR scenes over the Central Business District of the city of Perth in Australia. The results are compared to a conventional algorithm.

1. Introduction

Persistent Scatterer Interferometry (PSI) enables to monitor the displacement of the surface and other backscatter points in urban areas from a stack of SAR acquisitions. It was introduced in [3] and works by decomposing the main

---

* Corresponding author. Tel.: +49721 608 46994
   E-mail address: matthieu.rebmeister@kit.edu

components of the interferometric phase, in order to reconstruct the height, the linear displacement rate and the thermally induced displacement of the potential dominant scatterer in a SAR pixel. Due to the side looking geometry of SAR acquisitions, it is possible that there are two or more dominant scatterers at different heights within a resolution cell. The reconstruction of those multiple PS-points is the goal of PS tomography, which estimates the number and intensity of dominant scatterers in a resolution cell along with their respective height, linear deformation rate, and eventually seasonal motion or thermal dilation. As the signal is assumed to be sparse in the elevation direction, it can be advantageous to use Compressive Sensing methods to solve the problem.

This paper presents a new algorithm to detect the different parameters of PS-points by using the orthogonal matching pursuit as a first Compressive Sensing approximate solution, and then least squares in order to further improve the estimation.

2. PSI and Tomographic Estimation

For the rest of the article, some assumptions are made:
- the reference phase and the topographic phase using a global Digital Elevation Model (DEM) are already removed.
- all the scenes are coregistrated to a single master.
- only small urban areas are considered, where atmospheric phase components and other large-scale variations are small enough
- phase contributions which can be modeled as a linear function of certain parameters are predominant

The Persistent Scatterer Interferometry enables the analysis from large areas by separating the different phase components of the dominant scatterer in a resolution cell. The goal is to find multiple parameters associated with a SAR pixel, as the residual height, the linear displacement rate or the thermal displacement, using a stack of $N+1$ SAR scenes. The classic model used for one interferogram is described in Equation 1 and contains ϕ_h which is due to the local residual height with respect to the DEM, ϕ_v due to the linear displacement of the PS, ϕ_α due to the thermal displacement of the PS and ϕ_{atmo} is due to atmospheric change between the master and slaves acquisitions.

$$\phi = \phi_h + \phi_v + \phi_\alpha + \phi_{atmo} + \phi_{noise} \tag{1}$$

There is a linear relation between the three first phase components and the parameter to be found, which are detailed in Equation 2.

$$\phi_h = -\frac{-4\pi}{\lambda}\frac{B_\perp}{r\sin(\theta)}h \ ; \ \phi_v = -\frac{-4\pi}{\lambda}\frac{B_t}{365}v \ ; \ \phi_\alpha = -\frac{-4\pi}{\lambda}B_K\alpha \tag{2}$$

$B_\perp$ in is m the orthogonal baseline between the master and the slave, B_t is the number of days between the master and the slaves and finally B_K is the temperature difference in K. h is the height in m, v is the linear displacement rate in m/y and α is the thermal displacement rate in m/K. It is important to remember that the measured phase is wrapped, which turns all those linear problems into a non-linear one. There are several different approaches in order to solve this problem. The most efficient and known methods are Ferretti's approach [3], StaMPS [6], where only the height is estimated before the unwrapping, SBAS [1], M-SBAS [8]. After the estimation of the parameters, it is important to validate if the values found are correctly estimated. The main criterion used is the temporal coherence γ_{PS}, computed as follows:

$$\gamma_{PS} = \frac{1}{N}\left|\sum_{n=1}^{N}\exp(i(\phi_n - \hat{\phi}_n))\right| \tag{3}$$

where ϕ_n is the observed phase at n^{th} interferogram and $\hat{\phi}_n$ is the reconstructed phase with the estimated parameters.
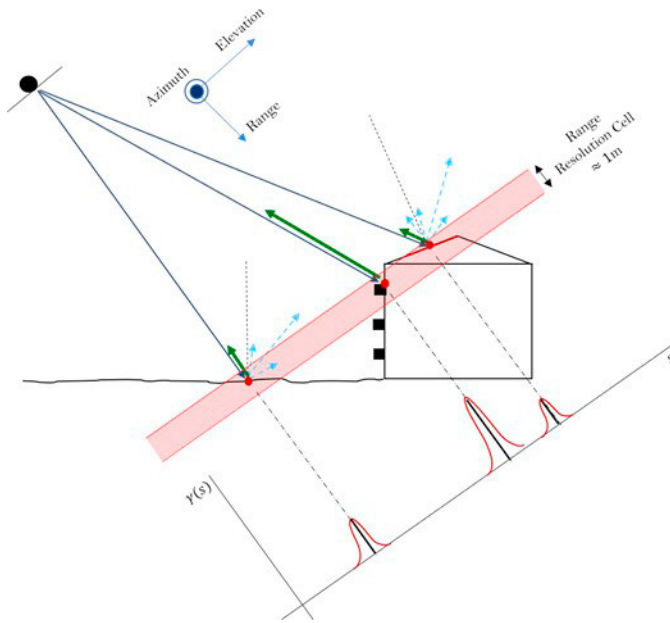
Figure 1: Illustration of the Tomographic Reconstruction

Tomographic reconstruction works with the complex signal in order to reconstruct the reflectivity profile in elevation direction. The first demonstration of TomoSAR was made in [7]. It enables to find more than one scatterer in a resolution cell, as can be seen in Figure 1.

However, the main problem in Tomo-SAR is the high computation time. In [2], a PSI and tomographic solution were compared. While the first one presented a smaller number of PS, the computation time required was 60 times larger for the tomographic approach.

A well-known TomoSAR algorithm is SL1MMER (Scale-down by L_1- Minimization, Model selection and Estimation Reconstruction) which is based on Compressive Sensing optimization methods. Given a set of interferometric measurements $\mathbf{g}$, the reconstruction of the reflectivity profile $\boldsymbol{\gamma}$ is possible via the inversion of the matrix $\mathbf{L_h}$ which links the two quantities.

$$\mathbf{g} = \mathbf{L_h}\boldsymbol{\gamma} \tag{4}$$

$$(\mathbf{L_h})_{p,q} = \exp\left(-i\frac{4\pi}{\lambda} \frac{B_{\perp,p}}{r\sin(\theta)} h_q \right) \tag{5}$$

In Equation 5, λ is the wavelength of the signal, r is the range between the satellite and the center of the scene, θ is the look angle, $B_{\perp,p}$ is the orthogonal baseline of the p-th interferogram and h_q is the discretized height. Using a classical master-slave configuration and a fine discretization step in the elevation direction, there are more columns than rows which means that there are more unknowns than measurements. An additional information is that the signal is sparse in the elevation direction, as it is almost impossible that there are more than four dominant and coherent points in a resolution cell according to [12]. It confirms that Compressive Sensing methods can be used.

The goal of Compressive Sensing is to solve Equation 4 using the sparsity prior knowledge which can be translated by solving the following problem:

$$\text{minimize}\left\{ \left\| \mathbf{L}\boldsymbol{\gamma} - \mathbf{g} \right\|_2^2 + \Lambda \left\| \boldsymbol{\gamma}_1 \right\| \right\} \tag{6}$$

where Λ is the regularization parameter. Theoretically, the norm which enforces sparsity is the $\| . \|_0$-norm but leads to an NP-hard problem. The $\| . \|_1$-norm is the convex relaxation of the problem. With this it is possible to solve the problem by using convex optimization algorithms, as the Basis Pursuit DeNoising (BPDN) approach in the original version of SL1MMER or more recently the Randomized Blockwise Proximal Gradient (RBPG) [9], which is faster.

3. Simultaneous vs. sequential Parameter Estimation

The goal of the developed algorithm is to reconstruct the parameters of the dominant scatterers in the pixel, which are given by the following observation equations for the n-th interferogram.

$$g_n = \sum_{j=1}^{Q} \gamma_j \cdot \exp\left(-i\frac{4\pi}{\lambda}\frac{B_{\perp,n}}{r\sin(\theta)}h_j\right) \cdot \exp\left(-i\frac{4\pi}{\lambda}\frac{B_{t,n}}{365}v_j\right) \cdot \exp\left(-i\frac{4\pi}{\lambda}B_{K,n}\alpha_j\right) \tag{7}$$

There are $3Q + 1$ parameters to estimate: the residual height, the linear displacement rate and the thermal dilation for each scatterer in the resolution cell, plus Q which is the number of significant scatterers in the resolution cell. The matrix $\mathbf{L_h}$ from Equation 5 is used to estimate the height. For the two other parameters, linear displacement rate and thermal dilation, the respective following matrices are used:

$$(\mathbf{L_v})_{p,q} = \exp\left(-i\frac{4\pi}{\lambda}\frac{B_{t,p}}{365}v_q\right); (\mathbf{L_\alpha})_{p,q} = \exp\left(-i\frac{4\pi}{\lambda}B_{K,p}\alpha_q\right) \tag{8}$$

$B_{t,p}$ is the temporal baseline and $B_{K,p}$ is the thermal baseline, which means the difference of temperature at the ground between the acquisitions. In M-SBAS, the estimation is done with stacks of small-baseline interferograms selected from all $\frac{N(N-1)}{2}$ possible interferometric combinations and by decomposing the 3D-parameter estimation into a sequential and iterative 3x1D-parameter estimation approach in order to reduce computation time [8]. By using arbitrary and variable interferogram stacks, including slave-slave interferograms for each parameter, and by using a sequential estimation approach, M-SBAS is limited to conventional single PS estimates with $Q + 1$.

The other possibility is to solve the problem in the 3D-space using a combination of the three matrices presented in Equation 5 and 8. The Kronecker product is the intuitive way to combine such measurement matrices, for example when the multi-dimensional problem can be interpreted as an image (2D) or a video (3D). In the encountered case, there are only N measurements in the classical master-slave configuration, and the number of rows of the measurement matrix should not increase by estimating three parameters, which would be the case by using the Kronecker product with the measurement matrices, namely N^3 rows. That is why the transposed Khatri-Rao product • was implemented and works as follows:

For $\mathbf{A} \in \mathrm{M}_{p\times r}(\square$ and $\mathbf{B} \in \mathrm{M}_{p\times s}(\square$, $\mathbf{B_i}$ denotes the *i*-th row of the matrix $\mathbf{B}$

$$\mathbf{C} = \mathbf{A} \bullet \mathbf{B} = \begin{pmatrix} a_{11}\mathbf{B_1} & \dots & a_{1r}\mathbf{B_1} \\ a_{21}\mathbf{B_2} & \dots & a_{1r}\mathbf{B_2} \\ \vdots & \vdots & \vdots \\ a_{p1}\mathbf{B_p} & \dots & a_{pr}\mathbf{B_p} \end{pmatrix} \subset \mathrm{M}_{p\times rs}(\square \tag{9}$$

So, the final measurement matrix is given as:

$$\mathbf{L} = \mathbf{L_h} \bullet \mathbf{L_v} \bullet \mathbf{L_\alpha} \tag{10}$$

This product can combine the three matrices. The output matrix is smaller than the conventional Kronecker product, but still very large and the computation time will have time-complexity of $\mathcal{O}(N^d)$, where d is the number of parameters to estimate. However, it avoids the iterative estimation and provides a basis for a multi-dimensional Compressive Sensing estimation approach.

4. Proposed Method

4.1. Parameter Estimation

The proposed method is based on a greedy Compressive Sensing algorithm: the Orthogonal Matching Pursuit (OMP). It works completely differently than the optimization method used in SL1MMER. Indeed, greedy algorithms are faster

but also less accurate than the optimization methods. More information about the different types of Compressive Sensing algorithms can be found in [4].

The disadvantage of greedy methods over optimization methods, as the classical BPDN, is that the number of points in the resolution cell must be given as a prior knowledge, which is not available in SAR Tomography. Thus, the algorithm must be tested for one, two or three etc. potential PS in the resolution cell, whereas the optimization methods do not need this additional parameter. However, the ill-posed configuration of the acquisitions leads to a high coherence for the matrix $\mathbf{L_h}$ and induces some artefacts in the reconstruction of the elevation profile. In SL1MMER, the Bayesian Information Criterion (BIC) is used in order to delete those artefacts and select the optimal number of scatterers in the resolution cell. With a greedy method, the only thing to do is to select the most plausible number of PS in the pixel because no artefacts are reconstructed.

The chosen greedy algorithm is the OMP and is introduced in [10]. It was selected among the L_1-minimization, CoSaMP, and the Fast Hard Thresholding Pursuit (FHTP), as the best compromise with respect to accuracy and speed. This selection was done based on simulations with single and double scatterers. In order to speed up the solution, the choice was made to perform a two-step OMP with a first coarse discretization step over a large range of possible values, and then on a finer grid, nested around the first results to increase the accuracy of the results.

The OMP is a well-known algorithm to provide approximate solutions of the problem. After the run of the OMP for each assumed number of scatterers in the pixel, the number of unknowns was considerably reduced. From more than a thousand unknowns which correspond to the values of the reflectivity profile, there are only 4 unknowns per PS after this step: reflectivity, height, linear displacement rate, and thermal dilation, for which the OMP gives approximate solutions. These values are used for the first iteration of a Least Squares estimation via the Gauß-Markov Model. With the decomposition of the complex exponential in trigonometric functions, it is possible to rewrite the model of the signal in Equation 7 as follows:

$$g_n = \sum_{j=1}^{Q} \gamma_j \cdot \left[\cos\left(C_{h,n}h_j + C_{v,n}v_j + C_{\alpha,n}\alpha_j + \phi_d\right) + i\sin\left(C_{h,n}h_j + C_{v,n}v_j + C_{\alpha,n}\alpha_j + \phi_d\right) \right] \quad (11)$$

The three coefficients C represent the factor for each unknown and depend on the baseline (cf. Equation 2). An additional unknown is added which is ϕ_d and represents the residual phase of the master acquisition, like neutrospheric phase delay, that is present in all interferograms.

The separation of the real part and the imaginary part of the equation gives the two following real equations.

$$R_n = \sum_{j=1}^{Q} \gamma_j \cdot \cos\left(C_{h,n}h_j + C_{v,n}v_j + C_{\alpha,n}\alpha_j + \phi_d\right) = F_n(\gamma_j, h_j, v_j, \alpha_j, \phi_d) \quad (12)$$

$$I_n = \sum_{j=1}^{Q} \gamma_j \cdot \sin\left(C_{h,n}h_j + C_{v,n}v_j + C_{\alpha,n}\alpha_j + \phi_d\right) = F_{N+n}(\gamma_j, h_j, v_j, \alpha_j, \phi_d) \quad (13)$$

This means that with an initial set of N complex measurements, a set of $2N$ real measurements can be exploited. The derivations of the functions F_n, $n \in \llbracket 1 ; 2N \rrbracket$ are not difficult to compute as it is only a sum of trigonometric functions. These derivatives fill up the design matrix A_k at each step k.

Iteratively, the parameter estimation is done according to the following estimator (Equation 14) until a stopping criterion over the norm of $\mathbf{dx}$ or the number of iterations is met.

$$\mathbf{dx_{k+1}} = (\mathbf{A_k^* A_k})^{-1}(\mathbf{A_k^* dg_k}) \quad (14)$$

This final estimator has the advantage that it works only with real data and this is more suitable for the analysis of the covariance matrix $\mathbf{C}_{\hat{\mathbf{x}}\hat{\mathbf{x}}}$, which is in this case given at the final iteration by

$$(\mathbf{A}^*\mathbf{A})^{-1} = \mathbf{C}_{\mathbf{xx}} \tag{15}$$

4.2. PS Selection

After the estimation, a criterion must be established in order to select the most likely number of PS in a resolution cell, and to detect, if they really can be considered as PS-points or if they must be discarded. The chosen criterion is based on the coherence from [6], and the Information Criterion as the Bayesian or Akaike one and is called the Measure for Phase Stability (MPS). It is defined in Equation 16 and is denoted as γ_{MPS}.

$$\gamma_{MPS} = \max_k \left\{ \frac{1}{N} \left| \sum_{n=1}^{N} \frac{\hat{g}_{n,k}}{g_n} \frac{\|g_n\|}{\|\hat{g}_{n,k}\|} \right| - \beta(k-1) \right\} \tag{16}$$

where k represents the number of PS in the pixel. $\hat{g}_{n,k}$ is the estimated signal at interferogram n, using the values found during the estimation and injecting it into Equation 11. The quantity β is a free parameter and was determined empirically with simulated data. This parameter is very important because it has the same function as the BIC: discriminate a too big number of parameters. Our studies show an optimal value of 0.06.

Then, a series of three tests is provided to increase the quality of the results. They are only presented in the case when two scatterers were detected in order to simplify the notation, but it can be easily expended to the case of three scatterers. They are organized as follows:

- Test 1: It is based on the reflectivity ratio between the two scatterers. If $\frac{\max(\gamma_1,\gamma_2)}{\min(\gamma_1,\gamma_2)} > T$, then the smallest point is discarded, as it can not be really considered as a dominant scatterer over the second one. The value of T chosen is $T = 3$.
- Test 2: The difference between the OMP estimation and the LS estimation is computed for each parameter found. If it is larger than a given threshold for at least one of the parameters, it is assumed that the LS estimation has diverged and a third finer grid with the OMP is applied to replace the LS estimation
- Test 3: To ensure the quality of the double scatterers, a spatial topological test is applied. A ball is constructed around each point of the multiple PS with a given radius R. If there are no single scatterers in this ball, this component of the multiple PS is discarded. Indeed, even for perfect conditions and selected buildings in urban scenes, there are less than 30 percent of double-PS in the optimal case of Spotlight TSX data [12]. This means that the probability of single scatterers in the neighborhood of a double-PS is very high. If it is not the case, it means that the double PS is isolated, and the estimation is most likely erroneous. A relevant radius is $R = 30\,m$.

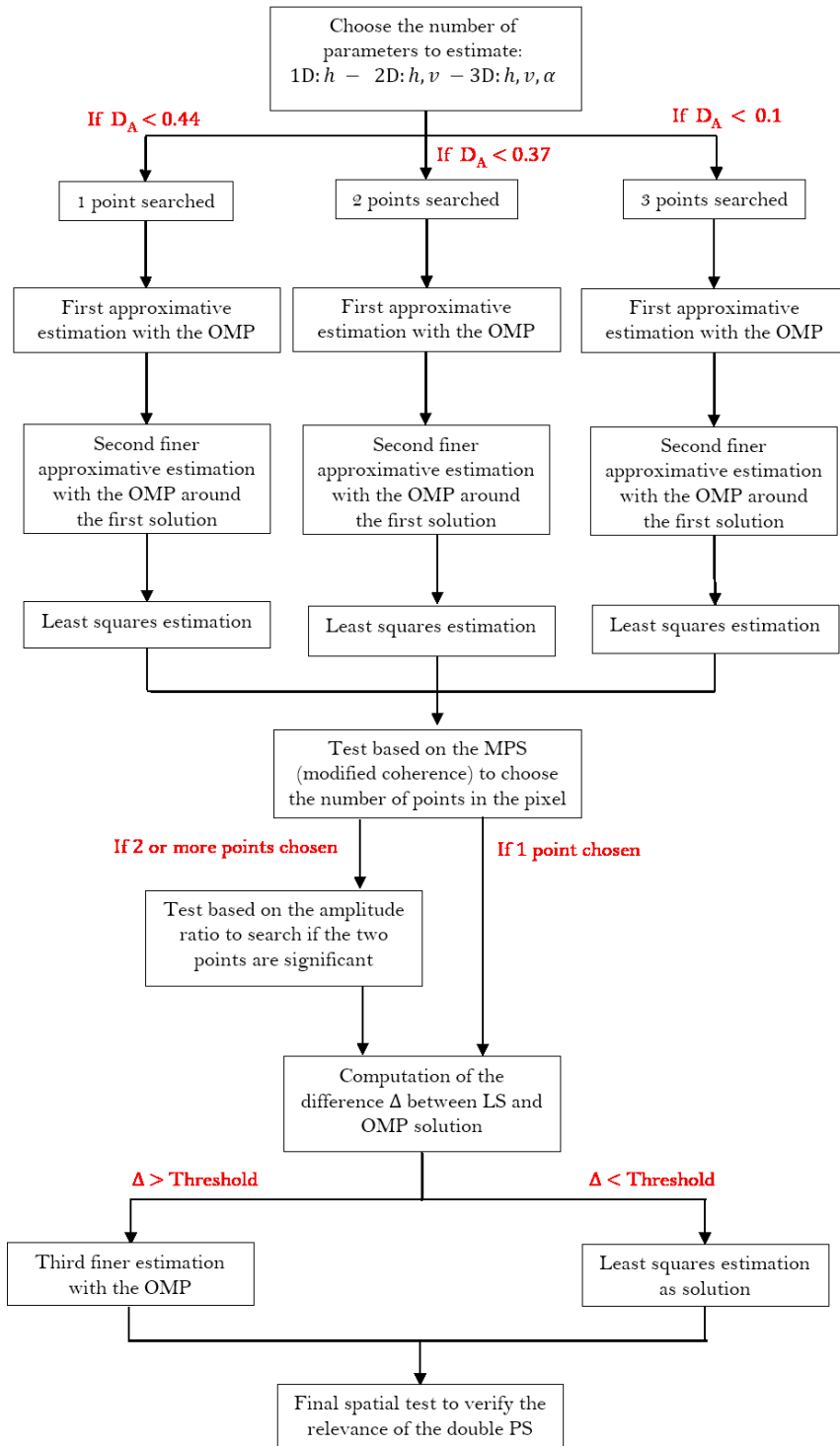The complete Flowchart of the Algorithm is given in Figure 2.

Figure 2: Flowchart of the proposed method

5. Application

5.1. Results on simulated data

The algorithm was first tested on simulated data, in order to tune the processing strategy and accurately assess the final estimation accuracy. The baseline configuration used to simulate data are from the Perth data stack which is further described in subsection 5.2. The theoretical resolution in height can be computed according to Equation 17

$$\rho_s = \frac{\lambda r}{2\Delta b}.$$ (17)

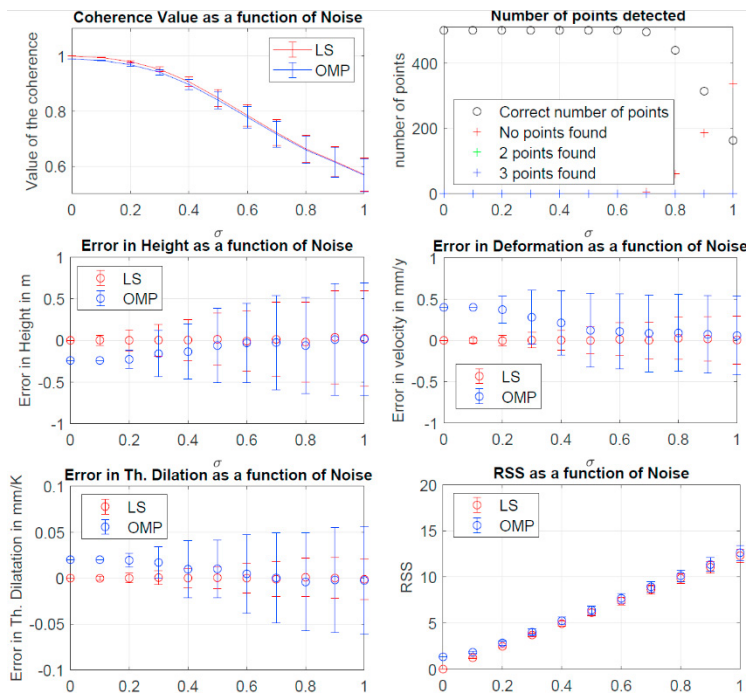For the used configuration, it is equal to $\rho_s = 10.9m$.

Figure 3: Analysis of the algorithm applied to the first case with only a single PS.

Three test cases are considered, presented in Table 1. The first case is the single PS case. Case 2 represents two scatterers in a SAR pixel which have the same reflectivity. Case 3 simulates two scatterers in the resolution cell which have a normalized distance of approximately 0.5. The normalized distance is the quotient of the real height difference between the points over the resolution in height ρ_s.

Figures 3, 4 and 5 show the results for the three scenarios. In all subfigures, the X-axis represents the increasing noise, for which the simulation were lead. It corresponds approximately to SNR from $+\infty$ to 0 dB. For each SNR, 500 PS-points were simulated with random circular Gaussian noise according to the SNR level.

In all subfigures of Figure 3, except for the upper right (UR) one, the blue curves represent the results after the OMP solution, whereas the red curves represent the results of 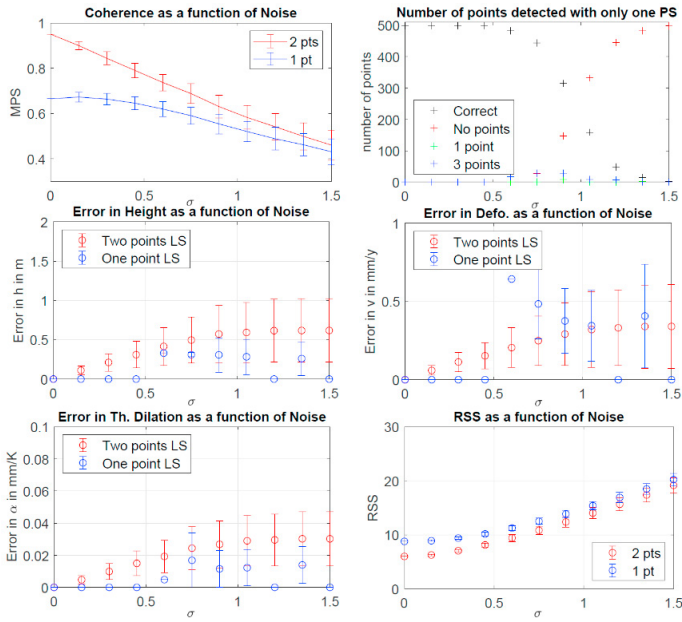the complete estimation. The LS estimation provides a significant improvement in the stability of the three parameters estimation (ML, MR, LL), which leads to an improvement of the coherence and the Residual Sum of Squares (UL, LR). Looking closer at the upper right graph, the number of detected points is always correct and avoids false alarms. With increasing noise, it starts to discard some points which is expected, considering the criterion used.

Table 1. Considered test cases with one or two PS per resolution cell with intensity $\gamma_{1/2}$, height $h_{1/2}$ in meter, linear displacement $v_{1/2}$ in mm/y and thermal dilation $\alpha_{1/2}$ in mm/K.

	γ_1	γ_2	h_1	h_2	v_1	v_2	α_1	α_2
Case 1	1.0	-	12.24	-	1.6	-	0.08	-
Case 2	1.0	1.0	4.56	25.34	-1.3	-1.6	0.09	0.24
Case 3	0.8	1.0	0.14	5.46	0.04	-1.2	0.00	0.05

Figure 4: Analysis of the algorithm, applied to the second case with two PS
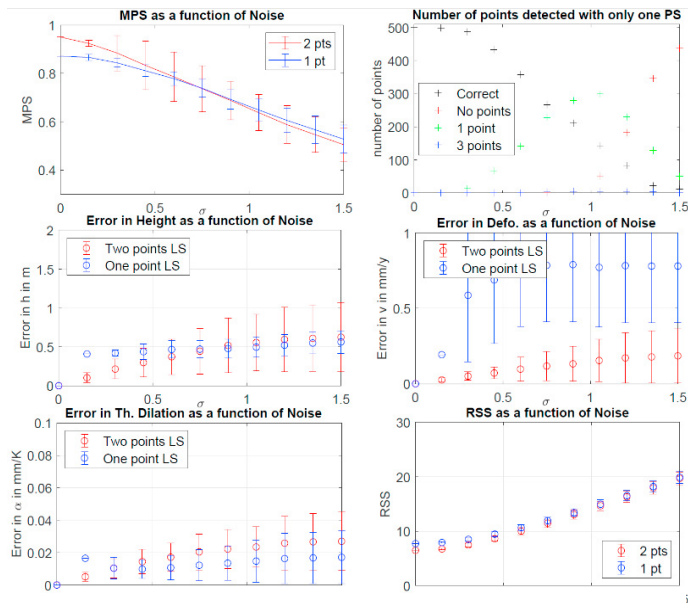
In Figure 4, the graph UL shows the mean MPS calculated with the respective standard deviation for each SNR in both detected scenarios: 1 PS or 2 PS estimated. It is clear that the MPS for two PS estimated is much higher than for only one PS. That is why the UR graphic shows that almost always the correct number of points is detected. The blue curves show the absolute error made when only one point was found, and the red curves represent the root mean square error for both reconstructed points. The errors have the magnitude order of what can be achieved with PSI or tomographic estimations. Indeed, the height error is about 0.5 m, the velocity error has a magnitude of 0.3 mm/y and the thermal dilation error is about 0.03 mm/K. The simulation represented in Figure 5 was simulated in order to analyze the super-resolution ability of the developed algorithm. It shows that with a low noise, it has good abilities to find both points. With increasing noise it finds more and more often only one point which is a mix of the two simulated PS. A surprising phenomenon is that the MPS is greater for one point than for two points when the noise becomes too large. This nicely demonstrates the preference of this algorithm towards sparse solutions. With high noise, it gives the same coherence to estimate the two separated points or one point in the middle.

The coefficient β in Equation 16 explains that the one PS case is selected more frequently. To conclude this section, the algorithm works very well for the single-PS case. In the case of multiple scatterers it works well too, but an almost 100% detection works only long with some restrictive assumptions, as a good separation of the scatterers and a reflectivity ratio reduced in a certain domain.

Figure 5: Analysis of the algorithm, applied to the third case with two PS

Table 2: Mean and standard deviation of the parameter estimation

X	h in m	v in mm/year	α in mm/K
$E(\hat{X}_{M-SBAS} - \hat{X}_{OCLeaS})$	0.20	0.01	0.01
$\sigma(\hat{X}_{M-SBAS} - \hat{X}_{OCLeaS})$	0.70	0.28	0.04

5.2. Test on a real data set

The test on simulated data was conclusive which invites us to use the method on a real data set. The choice was made to apply it on a stack of 79 TerraSAR-X Stripmap scenes over the Central Business District of Perth. These data present high skyscrapers possibly characterized by high thermally induced displacement rates, which renders the data interesting to test. The results are compared with M-SBAS, an alternative PSI-algorithm which uses the StaMPS framework but includes simultaneous estimation of height, displacement rate and thermal dilation in the PS selection process.
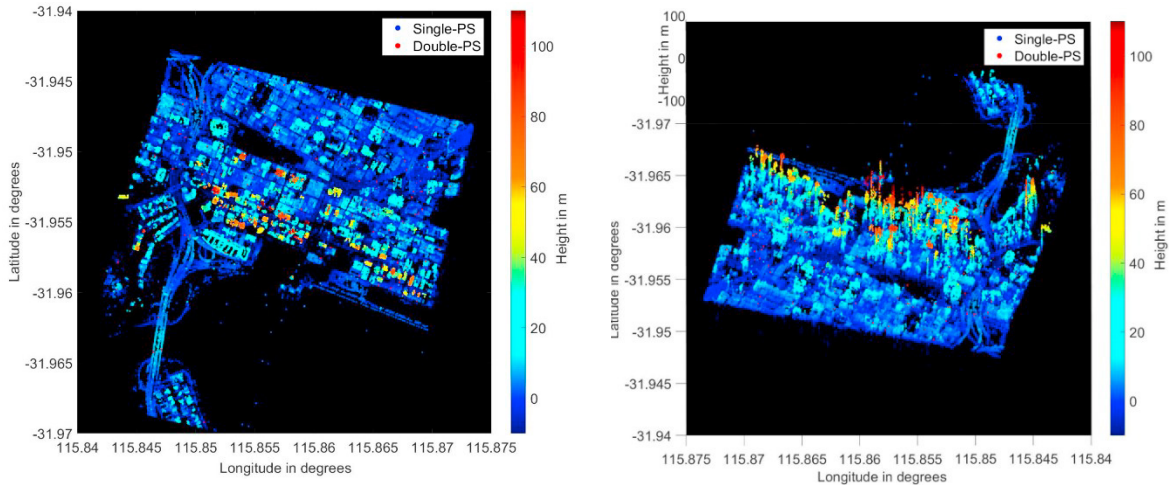

Figure 6: Visualization of the estimated height - 3D model of the CBD

The pixels considered as PS-Candidates are the pixels with an amplitude dispersion D_A smaller than 0.44. The reconstruction of the height with the proposed algorithm is given in Figure 6. The linear displacement rate and the thermal dilation are given in Figure 7. The mean linear displacement rate is quasi equal to 0 mm/y. In the areas circled in red, the displacement rate goes up to -5 mm/y. A test was made to use the algorithm only with the height estimation and in those areas, no PS-points are found. The number of double-PS found in the scene is quite low and represents 1% of the selected PS in the scene. According to [11], the utilization of SL1MMER can be up to 17% for Spotlight acquisitions. Also, it is important to notice that, unlike in our approach, in this study an additional preprocessing step is included to remove the atmospheric phase screen of the scene which increase the SNR and may improve the reconstruction of the reflectivity profile.

For each parameter $X, X = h, v, \alpha$, the mean $\mathbb{E}(\hat{X}_{M-SBAS} - \hat{X}_{OCLeaS})$ and standard deviation $\sigma(\hat{X}_{M-SBAS} - \hat{X}_{OCLeaS})$ are computed. It allows to statistically analyze the deviations to the M-SBAS estimation. For each parameter, the two quantities are summarized in Table 2. All the standard deviations are small w.r.t. the quantity evaluated. Indeed, the deviation of the height is about 0.7 m which is below the standard accuracy reached in SAR tomography of 1 m. The mean difference between M-SBAS and OCLeaS is negligible and can come from the local referencing, which is not identical.

6. Conclusion and Outlook

The proposed method enables an analysis of a stack of SAR scenes in order to monitor mainly urban areas. The comparison with a PSI algorithm shows similar results which is encouraging for future work. The use of the Khatri-Rao product allows to have a simultaneous estimation of all the parameters and seems to be adapted to a tomographic work. The next step of the work is the research on the acceleration of the estimation process, as the Khatri-Rao, for N points and d parameters to estimate, has a time-complexity of $\mathcal{O}(N^d)$. The tomographic reconstruction, especially the double scatterer identification works with simulated data but does not show the best efficiency on real data. The next

step which will be achieved is to compare the tomographic component with other Compressive Sensing algorithms like SL1MMER.
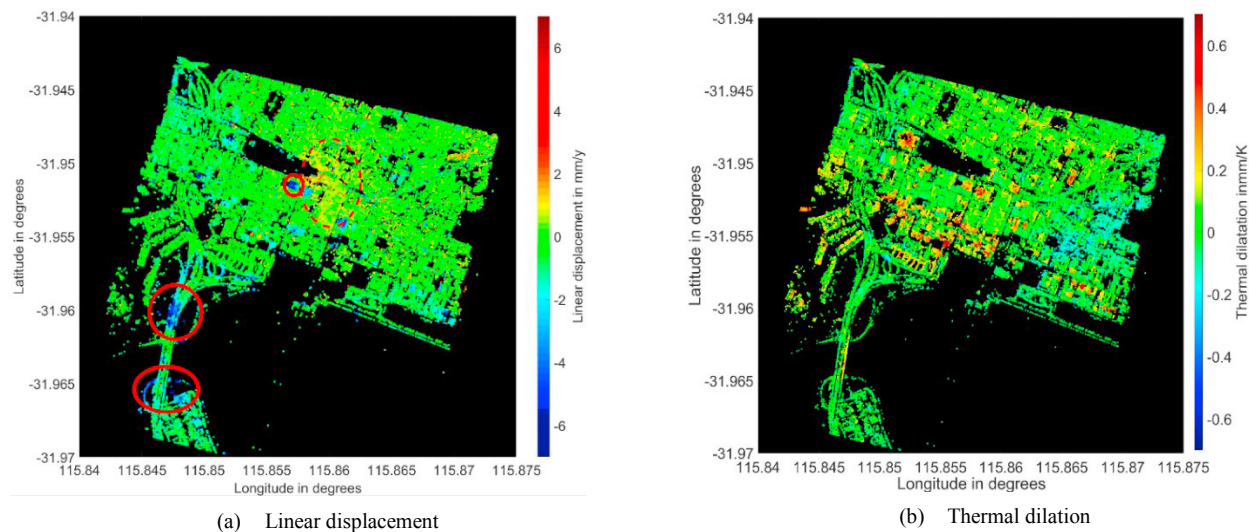

| (a)   Linear displacement | (b)   Thermal dilation |

Figure 7: Visualization of two 4D - models of the CBD

Acknowledgement

References

[1] Berardino P, Fornaro G, Lanari R, Sansoti E (2002) "A new algorithm for surface deformation monitoring based on small baseline differential SAR interferograms." *IEEE Transactions Geoscience and Remote Sensing* **40**: 2375-2383.

[2] Budillon A, Crosetto M, Johnsy AC, Monserrat O, Krishnakumar V, Schirinzi G (2018) "Comparison of Persistent Scatterer Interferometry and SAR Tomography using Sentinel-1 in urban environment" *Remote Sensing* **10** (**12**)

[3] Ferretti A, Prati C, Rocca F (2000) "Nonlinear subsidence rate estimation using permanent scatterers in differential SAR Interferometry" *IEEE Transactions, Geoscience and Remote Sensing*, **38**: 2202-2212.

[4] Foucart S, Rauhut H (2013) "A Mathematical Introduction to Compressive Sensing", Applied and Numerical Harmonic Analysis, Springer, New-York

[5] Hooper A, (2006) "Persistent Scatterer Radar Interferometry for Crustal Deformation", PhD Thesis, Stanford: Stanford University

[6] Hooper A, Segall P, Zebker H (2007) "Persistent Scatterer InSAR for crustal deformation analysis with application to Volcán Alcedo, Galapágos." *Journal of Geophysical Research*, 112.

[7] Reigberger A, Moreira A (2000) "First demonstration of Airborne SAR tomography using multibaseline L-band data." *IEEE Transactions Geoscience and Remote Sensing* **38 (5)**: 2142-2152.

[8] Schenk A (2015) "PS-Interferometrie in urbanene Räumen – Optimierte Schätzung von Oberflächenbeegungen mittels Multi-SBAS Verfahren" PhD Thesis, Karlsruhe Institute of Technology

[9] Shi Y, Zhu X, Yin W, Bamler R (2018) "A fast and accurate Basis Pursuit denoising algorithm with application to Super-Resolving Tomographic SAR" *IEEE Transactions, Geoscience and Remote Sensing*, **56**: 6148-6158

[10] Tropp JA, Gilbert AC (2007) "Signal Recovery from random measurements via Orthogonal Matching Pursuit", *IEEE Transactions on information theory*, **53 (12)**: 4655-4666

[11] Wang Y, Zhu X, Bamler R (2014) "An efficient tomographic inversion approach for urban maping using meter resolution SAR image stacks" *IEEE Geoscience and Remote Sensing Letters* **11 (7)**: 1250-1254

[12] Zhu X (2011) "Very High Resolution Tomographic SAR Inversion for Urban Infrastructure Monitoring – A sparse and non-linear tour", PhD Thesis, Technische Universität München.